Quaternary Science Reviews 284 (2022) 107493

Contents lists available at ScienceDirect

Quaternary Science Reviews

journal homepage: www.elsevier.com/locate/quascirev

Marine Isotope Stage 11c: An unusual interglacial

Polychronis C. Tzedakis [a, *], David A. Hodell [b], Christoph Nehrbass-Ahles [b], Takahito Mitsui [c, d], Eric W. Wolff [b]

[a] Environmental Change Research Centre, Department of Geography, University College London, London, UK
[b] Department of Earth Sciences, University of Cambridge, Cambridge, UK
[c] Earth System Modelling, School of Engineering & Design, Technical University of Munich, Munich, Germany
[d] Potsdam Institute for Climate Impact Research, Potsdam, Germany

ARTICLE INFO

Article history:
Received 22 November 2021
Received in revised form
11 March 2022
Accepted 26 March 2022
Available online 6 April 2022

Handling Editor: A. Voelker

Keywords:
Interglacial
MIS 11c
Insolation forcing
Sea level rise
CO_2
Ice sheets

ABSTRACT

Notoriety of the Marine Isotope Stage (MIS) 11c interglacial arises from its long duration, extending over two precessional cycles, high sea level, and persistence of high atmospheric CO_2 concentrations. The strong climatic response is often considered paradoxical because it was attained under weak boreal summer insolation forcing, a function of an extended eccentricity minimum and of precession and obliquity being almost opposite in phase. Here, we trace the characteristics of MIS 11c and explore their most likely causes. MIS 11c was preceded by the largest Quaternary ice volume expansion of MIS 12, which ended with a long period of ice rafting and interhemispheric heat transfer. We suggest that the duration of MIS 12 and the size of ice sheets exceeded a critical threshold that triggered a deglaciation despite the weak insolation forcing. The weak forcing led to a slow but steady loss of ice volume, that was sufficient to allow ocean outgassing of CO_2, but insufficient to raise sea level within a single precessional cycle. This gave rise to a prolonged interval with large residual ice sheets and high CO_2 concentrations that is unique in the last 800,000 years. The obliquity-precession antiphasing produced a weak boreal summer insolation minimum, skipping a glacial inception and leading to continued sea-level rise and high CO_2 concentrations, sustained by carbonate compensation. Full interglacial conditions were achieved in the second precessional cycle, and the combined strength and length of the interglacial probably led to loss of some Greenland and Antarctic ice compared to other interglacials. While MIS 11c is highly unusual in many respects, these appear to be linked to each other through the very weak insolation forcing, which led to its extended duration, slow sea-level rise and stable CO_2 concentrations through a cocktail of counteracting carbon cycle processes. Although some of these features are also encountered in other interglacials, their combination with strong interglacial intensity is unique to MIS 11c and this appears to be a function of the large MIS 12 ice sheets and the high CO_2 concentrations from the beginning of the interglacial.

1. Introduction

The interglacial within MIS 11, usually denoted as MIS 11c (~426–396 thousand years ago [ka]),[1] was one of the most prominent Quaternary interglacials (Fig. 1). It is the first interglacial following the so-called Mid-Brunhes Event (MBE), ushering in an era of higher amplitude glacial cycles and warmer interglacials with higher atmospheric CO_2 concentrations (Jansen et al., 1986; Berger and Wefer, 2003; Tzedakis et al., 2009; Barth et al., 2018). Its duration, approaching 30 thousand years (kyr), exceeds that of most Middle and Late Pleistocene interglacials (McManus et al., 2003; Tzedakis et al., 2012a) by at least 10 kyr. Comparisons of reconstructed peak sea surface temperatures (SST) and global average surface temperatures show that MIS 11c was, at its maximum, the second warmest interglacial behind the Last Interglacial (MIS 5e) during the last 800 kyr (Pages Working Group on

* Corresponding author.
E-mail address: p.c.tzedakis@ucl.ac.uk (P.C. Tzedakis).

[1] Railsback et al. (2015) introduced two additional Marine Isotopic Substages (11d and 11e) in the earliest part of MIS 11. Unlike well-defined Substages (such as MIS 5a-5e), characterized by substantial benthic $\delta^{18}O$ change and duration (usually about half a precession cycle), the MIS 11d and 11e of the Railsback et al. (2015) scheme represent brief minor inflections in the $\delta^{18}O$ curve of the benthic LR04 stack (Lisiecki and Raymo, 2005). Here, we therefore designate MIS 11c to extend to the base of MIS 11, which according to the definition of Tzedakis et al. (2012a), corresponds to the end of the 'terminal' oscillation of the bipolar seesaw.

https://doi.org/10.1016/j.quascirev.2022.107493

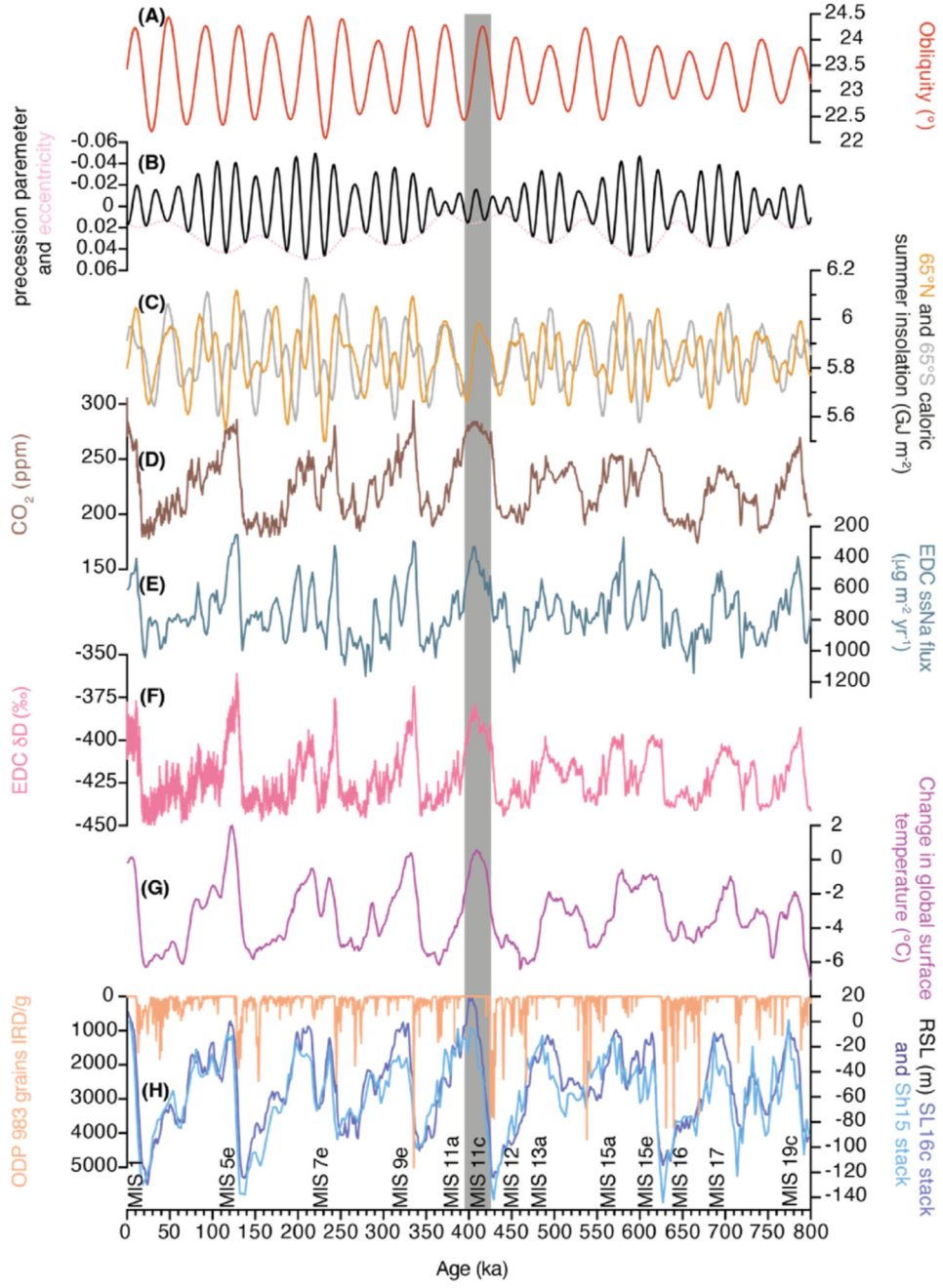

Fig. 1. Changes in climate conditions over the last 800 kyr. (A) Obliquity (Laskar et al., 2004). (B) Eccentricity (dashed) and precession parameter (Laskar et al., 2004). (C) Caloric summer half-year insolation at 65°N (orange) and 65°S (grey) (Laskar et al., 2004). (D) Compilation of atmospheric CO_2 records from Antarctic ice cores (Bereiter et al., 2015, and references therein; Nehrbass-Ahles et al., 2020; Shin et al., 2020; Bauska et al., 2021). (E) Sea salt Na flux in EPICA Dome C ice core, Antarctica (Wolff et al., 2006). (F) δD of ice in EPICA Dome C ice core, Antarctica (Jouzel et al., 2007). (G) Global average surface temperature as temperature deviation from present (average over 0–5 ka) (Snyder, 2016). (H) Ice rafted detritus (IRD) in North Atlantic ODP Site 983 (Barker et al., 2019 [salmon]); relative sea-level (RSL) reconstructions: sea-level stack combining multiple sea level records (Spratt and Lisiecki, 2016 [dark blue]) and planktic Foraminifera stack (Shakun et al., 2015 [light blue]). Ice core data plotted on the AICC2012 timescale (Bazin et al., 2013). (For interpretation of the references to colour in this figure legend, the reader is referred to the Web version of this article.)

Past Interglacials, 2016; Snyder, 2016). Sea-level reconstructions suggest a highstand of 6–13 m above present (Raymo and Mitrovica, 2012; Dutton et al., 2015) that may have exceeded that of MIS 5e, though other estimates place it closer to present level (e.g. Bowen, 2010; Rohling et al., 2010). A striking feature of MIS 11c is the prolonged persistence of relatively stable atmospheric CO_2 concentrations, hovering around 265–280 ppm for ~30 kyr (Nehrbass-Ahles et al., 2020) (Fig. 2E).

MIS 11c has traditionally been considered an astronomical analogue for the Holocene (Loutre and Berger, 2000, 2003). This similarity arises from the modulating effect of the 400 kyr eccentricity cycle on climatic precession, with low eccentricity leading to low-amplitude precessional changes and subdued seasonal insolation variations in both MIS 11c and the Holocene. However, whereas the Holocene contains one summer insolation peak, with the precession minimum and obliquity maximum occurring synchronously, MIS 11c extends over two insolation peaks, with precession and obliquity almost opposite in phase (Fig. 1A and B and

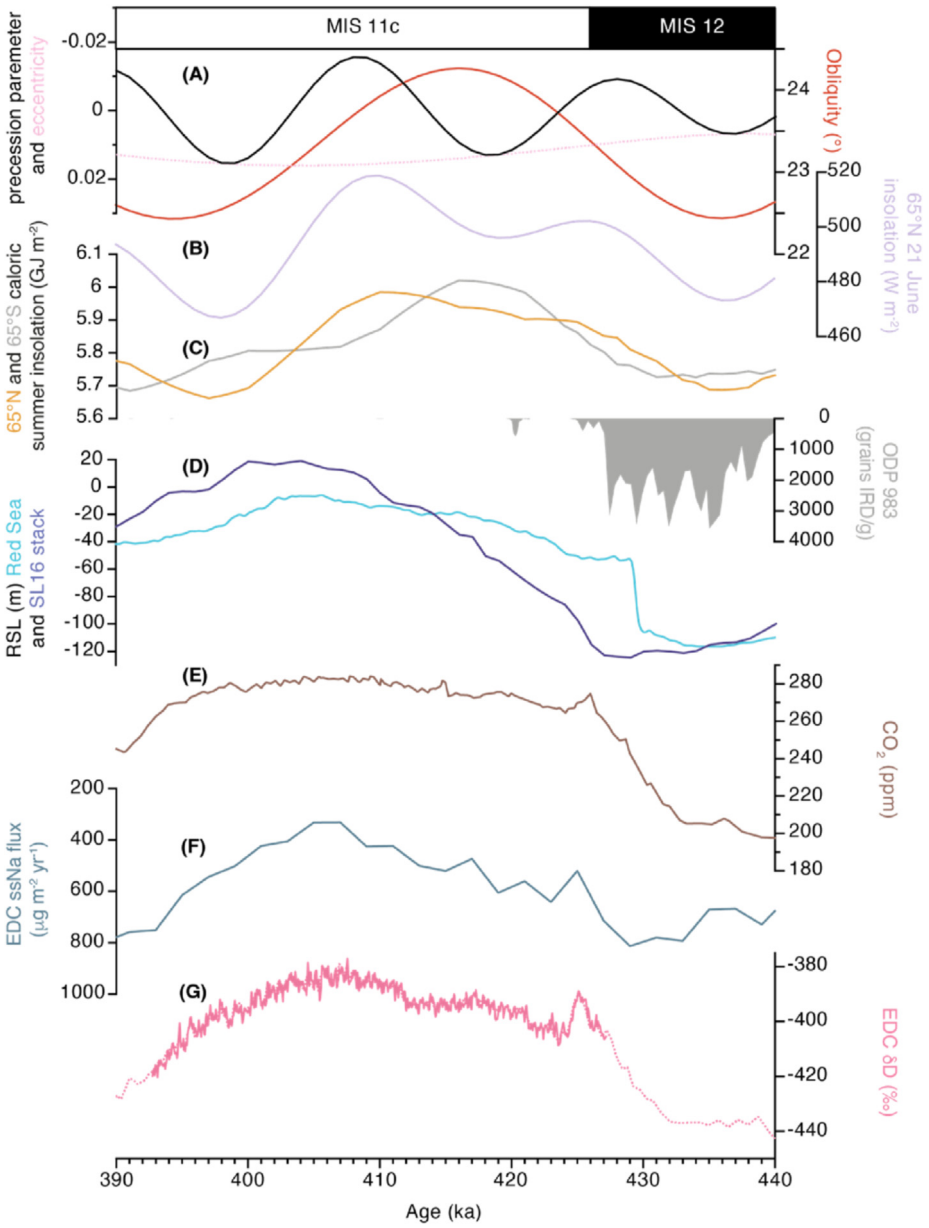

Fig. 2. MIS 11c climatic context. (A) Obliquity (red), eccentricity (dotted line) and precession parameter (black) (Laskar et al., 2004). (B) 21 June insolation at 65°N (Laskar et al., 2004). (C) Caloric summer half-year insolation at 65°N (orange) and 65°S (grey) (Laskar et al., 2004). (D) Ice rafted detritus (IRD) from North Atlantic Site ODP 983 plotted on the AICC2012 timescale (Barker et al., 2019 [grey filled curve]); relative sea-level (RSL) reconstructions: sea-level stack (Spratt and Lisiecki, 2016 [dark blue]) and Red Sea probability maximum RSL (Grant et al., 2014 [light blue]). (E) Atmospheric CO_2 in EPICA Dome C ice core, Antarctica (Nehrbass-Ahles et al., 2020). (F) Sea salt Na flux in EPICA Dome C ice core, Antarctica (Wolff et al., 2006). (G) δD of ice in EPICA Dome C ice core, Antarctica (Jouzel et al., 2007 [dashed line]; Pol et al., 2011 [solid line]). Ice core data plotted on the AICC2012 timescale (Bazin et al., 2013). (For interpretation of the references to colour in this figure legend, the reader is referred to the Web version of this article.)

2A). These differences impose limitations on the MIS 1–11c analogy and lead to divergent conclusions on the natural length of the current interglacial (Tzedakis, 2010; Tzedakis et al., 2012b). Despite these limitations, MIS 11c provides an observational context for climate processes and feedbacks that operate during periods of 'excess warmth' (e.g. Fischer et al., 2018).

Part of the ongoing fascination with MIS 11c is that it does not fit neatly into the astronomical theory of ice ages: the so-called 'Stage 11 problem' (Imbrie et al., 1993) derives from the disparity between the modest insolation forcing and the strong climatic response. In their 'Stage 11 Paradox', Berger and Wefer (2003) further noted that the MIS 12–11 transition has the largest range of Pleistocene climate variation, but only subdued insolation forcing. Despite accumulating evidence (see Droxler et al., 2003a; Candy et al., 2014), a number of issues remain outstanding: Why was there a deglaciation around 430 ka (known as glacial Termination V)? Why did sea-level rise slowly over the course of the interglacial and what was the effect of the slow deglaciation on regional climates? What led to the prolonged stability of CO_2 concentration? What were the implications of protracted interglacial duration? Was MIS 11c a 'super interglacial'? And finally, what is so special about MIS 11c? Here, we provide a synthesis of the current state of understanding and attempt to address these questions.

2. An improbable interglacial?

In essence, the 'Stage 11 problem' implies the implausibility of a glacial termination occurring at the MIS 12/11 transition under such modest insolation forcing. Indeed, a well-known feature of some conceptual model experiments is their difficulty in reproducing Termination V (e.g. Imbrie and Imbrie, 1980). The weak insolation forcing is a result of (i) a prolonged eccentricity minimum, leading to subdued precessional variations over the interval 460–360 ka (Fig. 1); and (ii) the obliquity maximum post-dating the first precession minimum by 12 kyr and preceding the second precession minimum by 8 kyr, which means that the summer insolation peak at 426 ka was not boosted by high obliquity (Fig. 2A–C).

Tzedakis et al. (2017) proposed that an interglacial onset occurs when a peak in summer insolation exceeds a deglaciation threshold that decreases with time elapsed since the previous interglacial onset. They also showed that while the sequence of Quaternary interglacials that has occurred is one among a very small set of possibilities, alternative histories might have arisen for a few cases where the effective energy was near the deglaciation threshold because of small differences in boundary conditions, solar or volcanic forcing and internal climate variability. In that scheme, MIS 11c was such a borderline case (Fig. 3A) and an alternatively scenario would have led to the skipping of MIS 11c and an interglacial onset at the summer insolation peak at 372 ka in MIS 11a (Fig. 1), as a result of a longer elapsed time since the MIS 13a deglaciation.

Underlying the concept of elapsed time in the scheme of Tzedakis et al. (2017) is the critical size of ice sheets in triggering deglaciations (e.g. Raymo, 1997; Paillard, 1998): over time the glacial system accumulates instability (MacAyeal, 1979) that makes ice sheets more sensitive to insolation increases, as a result of some combination of ice-sheet physics, glacio-isostatic adjustments, changes in ice-sheet albedo and ocean carbon storage (e.g. Birchfield et al., 1981; Ganopolski and Calov, 2011; Abe-Ouchi et al., 2013; Paillard and Parrenin, 2004). Foraminiferal isotope records suggest that MIS 12 was characterized by the largest ice volume expansion of the Quaternary (e.g. Shackleton, 1987; Elderfield et al., 2012). This is, in part, supported by glacial geological evidence for the large spatial extent of ice sheets in Europe (the Elsterian glaciation of continental Europe; the Anglian glaciation of the British Isles; the Okian glaciation of Russia) (Fig. 4), although locally this was not always the case (for example, the Elsterian glaciation was less extensive than the MIS 6 Saalian in western Germany and the Netherlands) (Hughes and Gibbard, 2018; Batchelor et al., 2019). However, the extent of the MIS 12 glaciation in North America (Illinoian D) remains weakly constrained (Batchelor et al., 2019).

In their summary of interglacials and glacials of the last 800 kyr, Lang and Wolff (2011) suggested that strong interglacials follow strong glacials. In the case of MIS 12, dynamic instability of the large ice sheets may have thus compensated for the modest insolation forcing at 426 ka, contributing to deglaciation. Thus, when elapsed time in the Tzedakis et al. (2017) model is replaced with estimates of sea-level lowstands based on the deconvolved oxygen isotopic composition of seawater (Elderfield et al., 2012), MIS 11c is no longer a borderline case (Fig. 3B). Indeed, Berger and Wefer (2003, p. 42) have argued that "Stage 11 was so warm, because Stage 12 was so cold". By extension, solving the 'Stage 11 problem' causes us to ask what led to the great MIS 12 ice sheets?

Raymo (1997) observed that major glacial terminations occur when significant 'excess' ice (defined as ~20–40 m sea-level equivalent [SLE]) has accumulated. This excess ice accumulates over intervals containing weak summer insolation maxima that only lead to minimal ice ablation, with the climate-cryosphere system continuing its trajectory towards increasingly larger ice sheets (Raymo, 1997; Paillard, 1998). Raymo (1997) further noted that terminations follow intervals of low eccentricity associated with such subdued precessional variations and ice accumulation. Hughes and Gibbard (2018) have therefore suggested that the large MIS 12 ice volume expansion may be related to the subdued eccentricity-precession forcing, which was further accentuated by the 400-kyr eccentricity cycle, over the interval ~450–430 ka (Fig. 1B). In addition, it is possible that the growth of large MIS 12 ice sheets was related to the presence of residual ice during the weak MIS 13a interglacial (e.g. Niu et al., 2021).

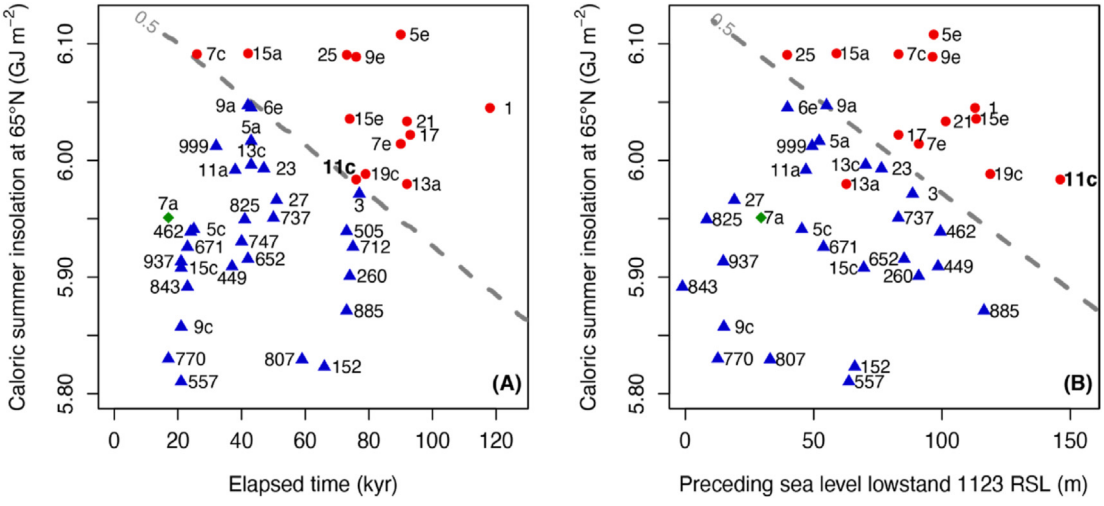

Fig. 3. Caloric summer half-year insolation peaks of the last 1 Myr against (A) time since the onset of the previous interglacial (Tzedakis et al., 2017); and (B) the preceding sea-level lowstand (from Elderfield et al., 2012) over the past one million years. Each point is an insolation peak. Red circles: insolation maxima nearest to the onset of interglacials; green diamond: continued interglacial; blue triangles: interstadials. Three-digit numbers represent ages, while all the other annotations are MIS numbers. The diagonal line separates insolation peaks associated with the onset of interglacials from those associated with a continued interglacial and interstadials over the past one million years and is derived as the 50th percentile of having an interglacial onset in a logistic regression model similar to that of Tzedakis et al. (2017). (For interpretation of the references to colour in this figure legend, the reader is referred to the Web version of this article.)

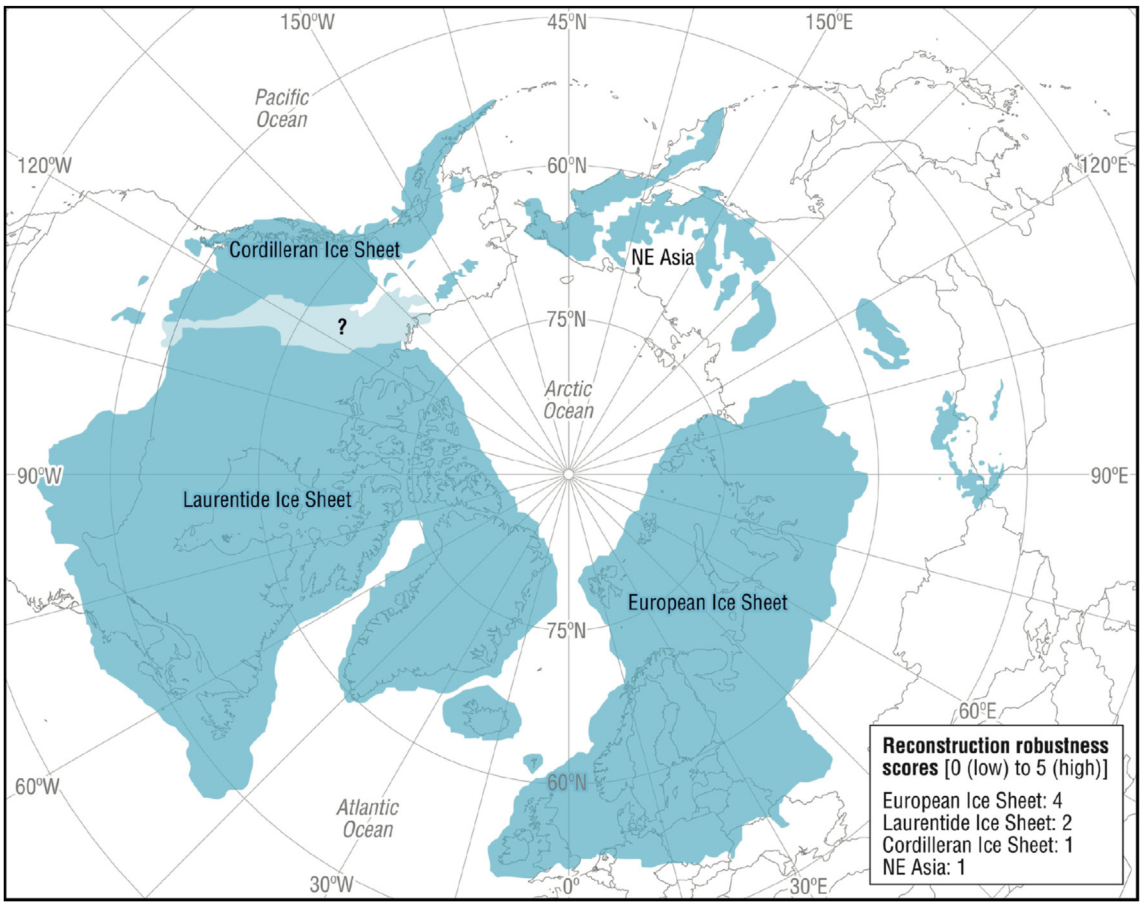

Fig. 4. Reconstructions of Northern Hemisphere ice-sheet extent (blue shading) during MIS 12 (429–477 ka) (modified from Batchelor et al., 2019). Ice-sheet robustness scores are also shown, reflecting a subjective assessment of the amount and reliability of the source data used in the reconstruction (see Batchelor et al., [2019] for further details). (For interpretation of the references to colour in this figure legend, the reader is referred to the Web version of this article.)

3. A staggered deglaciation

Ice rafted detritus (IRD) records from the North Atlantic show a long and prominent peak during the terminal Heinrich stadial preceding MIS 11c (Fig. 2D) (Oppo et al., 1998; Barker et al., 2015, 2019), a function of the large MIS 12 ice sheets along with the weak and slow increase in summer insolation. The freshwater influx promoted a weakening of the Atlantic meridional overturning circulation (AMOC), activation of the bipolar seesaw and interhemispheric heat transport. This in turn led to warming of Antarctica, as indicated by the parallel rise of δD values in the EDC Antarctic ice core Jouzel et al. (2007), Fig. 2G), and a likely contribution to sea-level rise from the wasting Antarctic ice sheet near the start of MIS 11c. The protracted warming of the Southern Ocean could also account for the extensive CO_2 outgassing from the Southern Ocean (Vázquez Riveiros et al., 2013), with atmospheric CO_2 concentration rising from 204 to 273 ppm between ~433 and 426 ka (Nehrbass-Ahles et al., 2020) (Fig. 2E).

In tandem with the prolonged operation of the bipolar seesaw, the relationship between the large MIS 12 ice sheets and deep-ocean salinity stratification may have also contributed to CO_2 outgassing from the Southern Ocean. More specifically, proxy evidence and modelling experiments suggest that the combined effects of large Northern Hemisphere ice sheets, low obliquity and low CO_2 under a glacial maximum state could strengthen the AMOC and cool the Southern Ocean remotely, leading to reduced melting of Antarctic land ice, enhanced equatorward sea-ice export and brine rejection, and the formation of very salty and relatively warmer Antarctic Bottom Water (AABW) (Adkins, 2013; Zhang et al., 2013; Galbraith and de Lavergne, 2019). This glacial deep-ocean stratification would decrease the potential cooling effect of waters upwelled in response to an AMOC weakening during a terminal Heinrich stadial, thereby amplifying the rate of Antarctic warming and potentially enhancing CO_2 outgassing from the Southern Ocean (Knorr et al., 2021).

In addition, the specific orbital configuration of Termination V may have contributed to CO_2 outgassing. Fig. 2C shows that both the caloric summer insolation at 65°N and at 65°S were rising during Termination V, a function of the weak eccentricity forcing. This minimized the influence of precession, whose impact is opposite across the two hemispheres, and led to rises in summer insolation at both polar regions under the influence of increasing obliquity. The increase in austral high-latitude insolation enhanced the melting of Southern Ocean sea-ice (Yin and Berger, 2012), as observed in the EDC sea-salt Na flux (Fig. 2F), a proxy for sea-ice extent (Wolff et al., 2006), allowing more CO_2 outgassing; a warmer Southern Ocean may have also destabilized the Antarctic Ice Sheet.

Unlike Terminations II, III and IV, which contain a pronounced millennial-scale overshoot in CO_2 concentrations followed by a monotonic decline (Fig. 1D), the early MIS 11c CO_2 concentrations show a small local maximum at 426 ka followed by a slight decrease over 1.7 kyr and then a slow rise over the next 15 kyr to ~280 ppm (Fig. 2E). Ganopolski and Brovkin (2017) have suggested

that pronounced CO_2 overshoots occur only when the AMOC remains suppressed for the entire deglaciation and recovers abruptly at the end of the meltwater flux (e.g. during Termination II [Deaney et al., 2017]). A protracted deglaciation would therefore not be expected to produce a pronounced millennial-scale CO_2 overshoot.

Indeed, despite differences in the estimated rate of sea level rise during Termination V (Rohling et al., 2010; Elderfield et al., 2012; Grant et al., 2014; Shakun et al., 2015; Spratt and Lisiecki, 2016; Giaccio et al., 2021), reconstructions agree that about 50–80 m SLE remained present in ice sheets near the start of MIS 11c (Fig. 2D). The early part of MIS 11c then saw a slow rise that took another ~20 kyr to reach maximum sea level. Reconstructions of global mean ocean temperature (MOT) from noble gases in the EPICA Dome C (EDC) ice core (Haeberli et al., 2021) imply a more gradual increase of MOT in MIS 11c (with a two-step build-up of MOT at the start and then in the middle of MIS 11c), unlike single-step increases in MIS 5e, 7e and 9e, but more measurements are needed to confirm this.

We suggest that the protracted deglaciation at Termination V arose from the unusual combination of weak eccentricity-precession forcing, precession-obliquity antiphasing and high CO_2 concentrations from the very start of MIS 11c. The obliquity peak at 416 ka (Fig. 2A) overrode the increase in precession and prevented any glacial inception associated with a decline in boreal summer solstice insolation (indeed the caloric summer half-year insolation, whose variance has equal contributions from obliquity and precession, does not decline at all). This was then followed by the second rise in boreal summer insolation, prolonging interglacial conditions (Tzedakis et al., 2012a).

4. A half-way house in early MIS 11c?

Thus, a curious situation arose during the first ~10–15 kyr of MIS 11c, with interglacial CO_2 concentration but with residual ice sheets persisting in the Northern Hemisphere (~50–80 m SLE at ~424 ka, and still ~20 m SLE at ~414 ka) (Fig. 2). Lower sea level in early MIS 11c would have maintained land bridges (e.g. between Britain and Europe [Candy et al., 2014]) or emergent low-lying areas (e.g. Sundaland (Brandon et al., 2020)) for much longer than in other interglacials. To emphasize the unusual nature of the early part of MIS 11c, we show the most extreme values of various parameters achieved during the periods containing the first (430–419 ka) and the second (419–398 ka) boreal summer insolation peaks (Table 1). The greenhouse gases (CO_2 and CH_4), as well as Antarctic temperature (represented by δD), show values in the first half of MIS 11c that are comparable to those of the stronger interglacials (including the Holocene). In contrast, sea level (Spratt and Lisiecki, 2016) and benthic foraminiferal oxygen isotopes (Lisiecki and Raymo, 2005) have values that are weaker than those of even the weakest interglacials of the last 800 kyr. In fact, if MIS 11c had ended at 419 ka, then it would, on sea level grounds, not have been considered an interglacial at all, and the conundrum would have been to explain how interglacial greenhouse gas concentrations could co-exist with glacial sea levels. It is this extended decoupling of the features we associate with interglacials – high CO_2 and high sea level (e.g. Tzedakis et al., 2009) – during the first period that is highly unusual; while a similar decoupling occurred during the early Holocene, it only lasted ~4 kyr (compared to ~20 kyr in MIS 11c). The lack of a strong summer insolation minimum at 419 ka allowed sea level rise to continue so that the second half of MIS 11c appears 'normal'. In all the parameters considered in Table 1, the strongest interglacial values occurred at or after the second summer insolation peak.

Apart from minor IRD events, subpolar North Atlantic records indicate a cessation of ice rafting in the early part of MIS 11c (Oppo et al., 1998; Barker et al., 2015), although the presence of small amounts of IRD in the Nordic Seas suggests that the Fennoscandian ice sheet had not yet retreated from the coastline (Kandiano et al., 2012). Benthic foraminiferal $\delta^{13}C$ values in the North Atlantic rose at the end of the terminal Heinrich stadial, ~426 ka (Fig. 5A), pointing to an increase in water ventilation and AMOC resumption (e.g. Hodell et al., 2008; Voelker et al., 2010; Vázquez Riveiros et al., 2013). The change in interhemispheric heat transport led to a concomitant cooling in South Atlantic surface conditions and Antarctic temperatures (Vázquez Riveiros et al., 2013). Reconstructions of SST show an abrupt warming at the start of MIS 11c in the mid/low latitude North Atlantic, but a delayed optimum in the Nordic Seas until after ~411 ka (Figs. 5B, S1, S2), a reflection of continued meltwater input and seasonal sea-ice expansion (Kandiano et al., 2012). This may also account for the gradual increase in benthic foraminiferal $\delta^{13}C$ records from the North Atlantic that peaked sometime between 410 and 400 ka (Fig. 5A), indicating a delayed maximum in North Atlantic Deep Water (NADW) production (Hodell et al., 2008; Oppo et al., 1998; Dickson et al., 2009; Voelker et al., 2010; Milker et al., 2013). While a global compilation of SST records, resampled at 1 kyr steps and normalized, shows a gradual increase during the course of MIS 11c, peaking near the second boreal summer insolation maximum at ~410 ka (Milker et al., 2013), higher resolution North Atlantic records reveal the presence of an early and late MIS 11c warm phases separated by a mid-MIS 11c cooling, with the final phase usually warmer than the first (e.g. Oppo et al., 1998; Stein et al., 2009; Rodrigues et al., 2011; Kandiano et al., 2012, 2017) (Fig. 5B; Fig. S1). A tripartite division is also observed in the MIS 11c compilation of atmospheric CH_4 concentration from the EDC ice core (Nehrbass-Ahles et al., 2020) and changes in the intensity of the Asian Monsoon from the Sanbao Cave speleothem record in China (Cheng et al., 2016), indicating coherent changes in low-latitude hydroclimate and tropical wetland extent (Fig. 5C and D). Isotopic constraints suggest only little change in the net source composition of atmospheric CH_4 over the course of MIS 11c (Bock et al., 2017). Pollen-based climate

Table 1
Most extreme values of different parameters achieved during the intervals containing the first (430–419 ka) and second (419–398 ka) boreal summer insolation peaks of MIS 11c.

	430-419 ka	Age (ka)	Comment	419-398 ka	Age (ka)
CO_2 (ppm)[a]	274	419	Similar to warm interglacials	282	409
CH_4 (ppb)[b]	707	422	Similar to warm interglacials	741	407
EDC δD (‰)[c]	−389	425	Similar to MIS 1 and MIS 19	−377	407.5
Sea-level stack (m)[d]	−51	419	Lower than any of MIS 1-19	16	404
LR04 $\delta^{18}O$ (‰)[e]	3.77	420	Higher than any of MIS 1-19	3.11	405

[a] Nehrbass-Ahles et al. (2020).
[b] Loulergue et al. (2008); Bock et al. (2017); Nehrbass-Ahles et al. (2020).
[c] Pol et al. (2011).
[d] Spratt and Lisiecki (2016).
[e] Lisiecki and Raymo (2005).

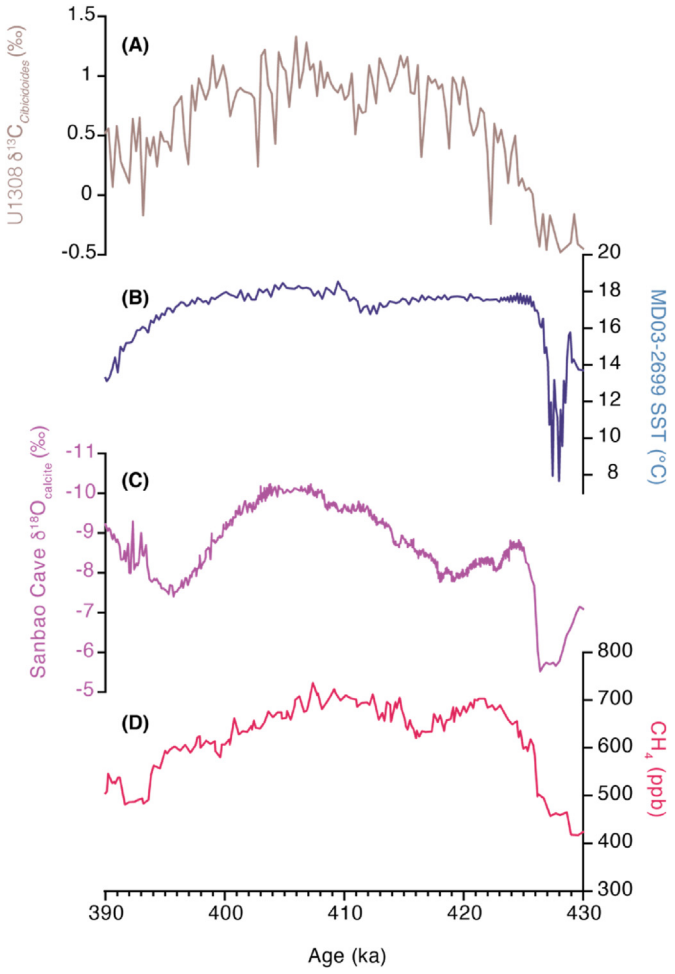

Fig. 5. MIS 11c climate records. (A) Benthic $\delta^{13}C$ record of *Cibicidoides wuellerstorfi* and/or *C. kullenbergi* from North Atlantic Site U1308 (Hodell et al., 2008). (B) Alkenone-based sea surface temperature record from MD03-2699 on the Portuguese Margin (Voelker et al., 2010). (C) Speleothem $\delta^{18}O$ record from Sanbao Cave, China (Cheng et al., 2016). (D) Compilation of atmospheric CH_4 (Loulergue et al., 2008; Bock et al., 2017; Nehrbass-Ahles et al., 2020) on the AICC2012 timescale (Bazin et al., 2013).

reconstructions from Lake El'gygytgyn in Siberia also show a tripartite MIS 11c division, but with the early phase as warm as the late (Melles et al., 2012). A strong warming in the earliest part of MIS 11c is also implied by speleothem growth in Ledyanaya Lenskaya Cave located in an area of mainly continuous permafrost in Siberia at 60°N, the last time that interglacial permafrost thawing occurred in that cave (Vaks et al., 2013, 2020). Possible causes for this early warming include reduced upwelling and stratification in northern North Pacific, ultimately related to reduction of Antarctic Bottom Water formation as a result of Antarctic ice sheet melting (Melles et al., 2012) and/or reduced sea-ice cover in the Arctic Ocean (Vaks et al., 2020). Speleothem evidence for permafrost thaw in MIS 11c has also emerged from a site in continuous permafrost area in the northern Yukon, but it is unclear whether this represents site-specific conditions or is part of large-scale thawing across the Arctic (Biller-Celander et al., 2021).

The picture that emerges for the early part of MIS 11c is therefore a complex mosaic of regional responses to an unusual combination of climate boundary conditions. The presence of residual ice sheets had a direct effect on high latitude air temperatures, as suggested by the delayed growth of temperate forest in central/northern Europe (e.g. Koutsodendris et al., 2010). However, the spatial distribution of these ice sheets and their recessive history in Europe and North America remain unconstrained. In the North Atlantic, the AMOC recovered at the start of the interglacial, but maximum NADW production was delayed until late MIS 11c. Protracted ice-sheet melting in the Nordic Seas led to a steep meridional SST gradient between the eastern subpolar and subtropical North Atlantic (Kandiano et al., 2012) and to a more southerly position of the Intertropical Convergence Zone in the first part of MIS 11c. This, combined with the weak boreal summer insolation peak at 426 ka, may account for the weaker increase in Asian Monsoon intensity in early MIS 11c relative to late MIS 11c indicated by the Sanbao speleothem record (Cheng et al., 2016). On the other hand, the small difference in absolute levels between the two peaks in CH_4 concentration (Fig. 5D) might point to additional emissions from the gradual flooding of low-lying areas (Ridgwell et al., 2012; Bock et al., 2017) and perhaps from high-latitude wetlands in early MIS 11c, as suggested by the Siberian temperature indicators (Melles et al., 2012; Vaks et al., 2020).

5. The carbon cycle and the persistence of high and stable atmospheric CO_2 concentration

MIS 11c is unusual in terms of the carbon cycle, which is marked by higher rates of coral reef (Droxler et al., 2003b; Husson et al., 2018), pelagic carbonate (Barker et al., 2006) and biosphere (Brandon et al., 2020) productivity. It is also part of the so-called Mid-Brunhes dissolution interval (~600–200 ka), when the lysocline and carbonate compensation depth (CCD) rose in response to increased removal of calcium carbonate ($CaCO_3$) from the ocean relative to input from rivers (Peterson and Prell, 1985; Farrell and Prell, 1989; Hodell et al., 2001, 2003; Qin et al., 2018). Several processes influenced atmospheric CO_2 during Termination V and MIS 11c, including CO_2 outgassing from the deep ocean, biosphere productivity, and reef and pelagic carbonate production (Kleinen et al., 2016). In turn, these transient changes in the carbon cycle elicited a steady-state response of the dissolved inorganic carbon (DIC) system known as carbonate compensation that is expressed as a change in deep-sea carbonate ion (CO_3^{2-}), leading to preservation or dissolution of $CaCO_3$ on the seafloor and atmospheric CO_2 change (Broecker et al., 1999).

In the deep South Atlantic and Indo-Pacific, a carbonate preservation event occurred when the lysocline and CCD deepened during Termination V and early MIS 11c (centred on ~425 ka) in response to outgassing of CO_2 from the deep ocean to the atmosphere (Fig. 6B,E). A peak in carbonate ion concentration occurs in the deep western tropical Pacific at this time (Qin et al., 2018). This was followed by reef growth during the slow sea-level rise over the next ~20 kyr. The relatively slow sea-level rise was conducive to reef productivity, which is estimated to have been greater during MIS 11c than in any other interglacial of the last million years (Husson et al., 2018). Similarly, biosphere productivity increased between 426 and 406 ka, and is estimated to have been 10–30% higher at the start of MIS 11c than at any subsequent interglacial, leading to a large uptake of atmospheric CO_2 (Brandon et al., 2020) (Fig. 6D). In early MIS 11c, terrestrial biosphere productivity may have been concentrated in tropical low-lying areas (e.g. Sundaland) that remained emergent due to the slow sea-level rise (Brandon et al., 2020) and perhaps areas of rapid warming in the Arctic (e.g. Melles et al., 2012). Later in MIS 11c, warm and wet conditions in mid-latitude areas (Candy et al., 2014; Kleinen et al., 2014) contributed to a major increase in forest biomass (e.g. Reille et al., 2000; Tzedakis et al., 2006). On the other hand, carbonate removal in reefs and pelagic carbonate (associated with a major increase in global coccolithophore production [Barker et al., 2006]) was a source of atmospheric CO_2 that countered the biosphere

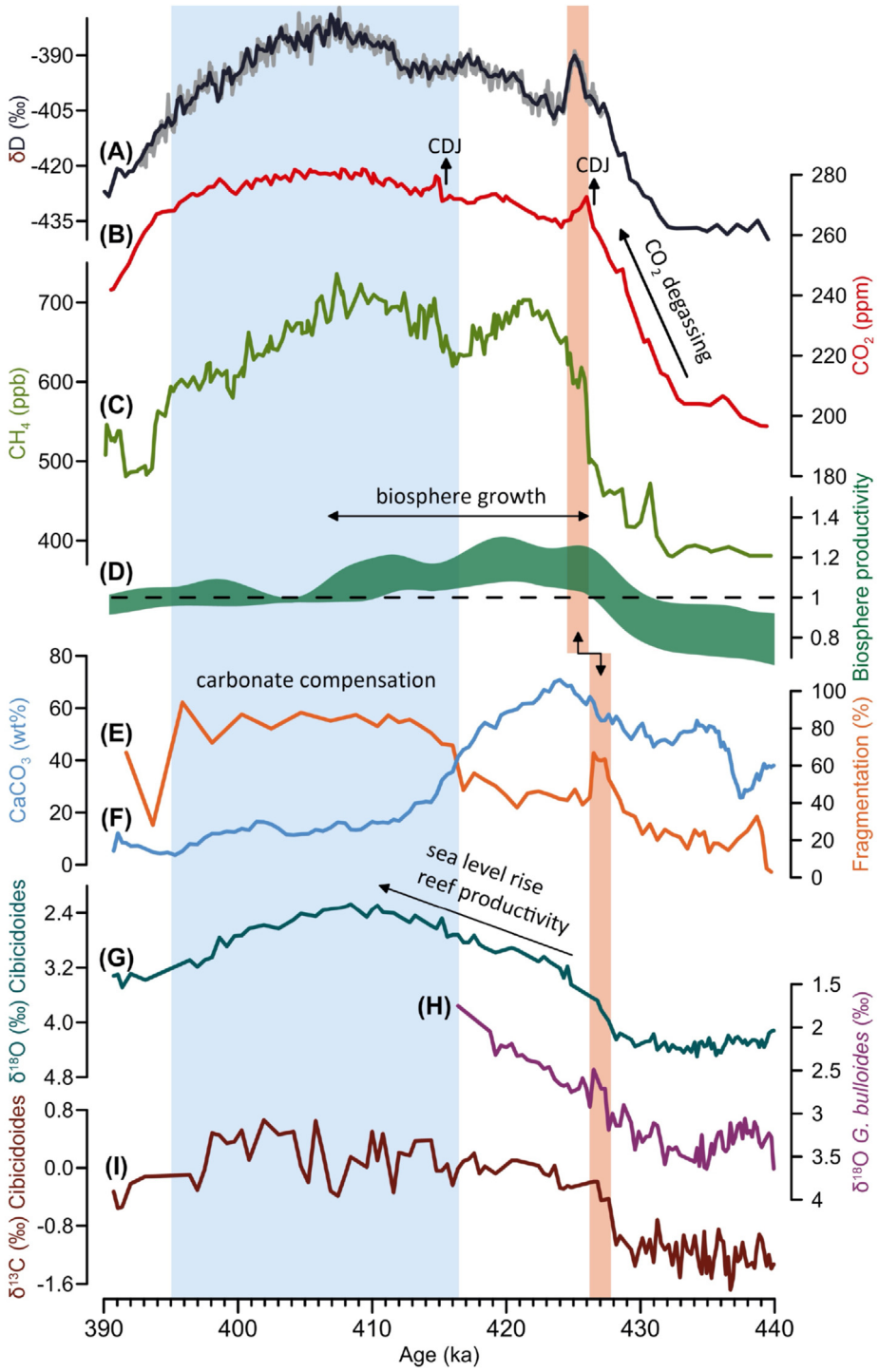

Fig. 6. Carbon cycle dynamics during MIS 11c. (A) δD of ice (Jouzel et al., 2007 [black]; Pol et al., 2011 [grey]). (B) Atmospheric CO_2 (Nehrbass-Ahles et al., 2020). (C) Compilation of atmospheric CH_4 (Loulergue et al., 2008; Bock et al., 2017; Nehrbass-Ahles et al., 2020). (D) Biosphere productivity based on $\Delta^{17}O$ measurements (Brandon et al., 2020). (E–I) Palaeoceanographic records from ODP Site 1089 in the deep South Atlantic (Hodell et al., 2001, 2003). (E) weight percent of calcium carbonate. (F) Percent fragmentation. (G) Benthic $\delta^{18}O$ of *Cibicidoides* species. (H) Planktic $\delta^{18}O$ of *Globigerina bulloides* (discontinuous record reflects the dissolution of planktic foraminifera). (I) Benthic $\delta^{13}C$ of *Cibicidoides* species. All ice core data were derived from the EPICA Dome C ice core and plotted on the AICC2012 timescale (Bazin et al., 2013). ODP 1089 data are on their original time scale (Hodell et al., 2003).

productivity sink. The shift in the locus of carbonate deposition from the deep-sea to shallow water resulted in a rise in the lysocline and CCD and carbonate dissolution in the deep ocean between ~415 and 392 ka (Fig. 6E). Carbonate ion in the deep Pacific plummeted from ~100 to 40 μ mol kg^{-1}, representing the greatest change over the last 700 kyr, (Qin et al., 2018). The lagged response of carbonate compensation would have led to an increase in atmospheric CO_2 during the latter half of MIS 11c. In parallel, however, the increase in coccolithophore production may have also led to CO_2 drawdown by strengthening the organic pump through

ballasting of organic matter from sinking coccoliths (Barker et al., 2006; Saavedra-Pellitero et al., 2017). Ultimately, because the time constant of carbonate compensation is long (with an e-folding time of ~6 kyr; Archer and Maier-Reimer, 1994), the effect was to prolong high CO_2 values, countering other processes tending to decrease it. It was only when carbonate compensation had restored the steady-state balance between DIC input from rivers and removal in the oceans that CO_2 began to decline.

MIS 11c also includes two periods when CO_2 rose abruptly on centennial timescales during interglacial conditions (Nehrbass-Ahles et al., 2020). The first Carbon Dioxide Jump (CDJ) marks the end of Termination V, giving rise to a local CO_2 maximum at 426 ka (Fig. 6B), comparable to Termination I (Marcott et al., 2014). A second CDJ formed at 415 ka, at a time of continued sea-level rise. This short-lived CDJ may be coeval with a cold event recorded in several North Atlantic sequences (Fig. S1), perhaps related to Greenland Ice Sheet melting and runoff leading to an AMOC perturbation, but timescale uncertainties and the lack of a highly resolved direct reconstruction of AMOC strength over MIS 11c complicate a direct attribution.

Finally, placing MIS 11c in a longer-term context, it remains unclear how its unusual carbon cycle is connected to the occurrence of the MBE and the shift towards stronger interglacials with higher CO_2 concentrations. Larger ice sheets may have contributed to more intense CO_2 outgassing from the Southern Ocean during terminal Heinrich stadials, but this is not always the case (for example, compare MIS 16-15e vs MIS 10-9e) (Fig. 1). Alternatively, the increase in post-MBE interglacial intensity has been attributed to an increase in the amplitude of obliquity cycles (EPICA community members, 2004), increased instability of the West Antarctic Ice Sheet (Holden et al., 2011) or weaker southern westerlies and Southern Ocean ventilation (Yin, 2013). After the MBE, weaker southern westerlies may have led to a reorganization of water masses in the Atlantic Basin and a reduction in the volume of interglacial AABW, contributing to a greater release of CO_2 from the deep ocean and warmer interglacials (Barth et al., 2018). However, the ultimate driver of this shift at the MBE remains elusive.

6. Effects of prolonged interglacial conditions

Climate – ice sheet modelling has suggested that the long MIS 11c duration was a necessary condition for the Greenland Ice Sheet (GrIS) to decline over several thousand years following the peak in summer temperature anomalies at the boreal summer insolation maximum 410 ka (Robinson et al., 2017). Marine sediment analyses off southern Greenland, using isotope and magnetic composition of subglacial silt, have been used to track the retreat of the southern GrIS during recent interglacials (Hatfield et al., 2016). During MIS 11c, these records show a period of ice melting, followed by the near cessation of ice-eroded sediment discharge, suggesting the near complete deglaciation of southern Greenland. This is supported by a marine pollen record off southern Greenland, indicating the presence of spruce forest in southern Greenland, with the maximum in spruce pollen values occurring near 400 ka (de Vernal and Hillaire-Marcel, 2008). Exposure-burial scenarios for the GISP2 bedrock core are consistent with GrIS reductions during MIS 11c (Schaefer et al., 2016). Taken together, geological constraints and ice sheet models suggest that GrIS may have contributed 4.5–6.1 m SLE to the MIS 11c sea-level rise (Reyes et al., 2014; Dutton et al., 2015; Robinson et al., 2017). Benthic foraminiferal $\delta^{13}C$ from the Eirik Drift off southern Greenland suggest a multi-millennial (~408–400 ka) interval of lower values that also contains an SST minimum and may reflect a disruption in NADW ventilation (Galaasen et al., 2020; Irvali et al., 2020). Beyond the immediate vicinity of Greenland, the impact of the partial deglaciation of the GrIS is unclear. Climate model experiments for MIS 11c (at 409 ka) show that the effect of removing GrIS entirely on surface air temperatures is limited to Greenland and environs (Coletti et al., 2015).

The MIS 11c history of the Antarctic ice sheets is weakly constrained. Sedimentary evidence from the Amundsen Sea is ambiguous about whether the West Antarctic Ice Sheet (WAIS) collapsed during the mid-Pleistocene, and if so, whether that occurred in MIS 11c (Hillenbrand et al., 2002, 2009). On the East Antarctic Ice Sheet (EAIS), subglacial opal and calcite precipitates in the Wilkes Subglacial Basin record a level of ^{234}U enrichment in MIS 11 that suggests major ice margin retreat with a potential contribution of 3–4 m to global sea level (Blackburn et al., 2020). This is consistent with sedimentological and geochemical evidence from a marine core offshore of the Wilkes Subglacial Basin, that shows the most extreme provenance changes during MIS 11 (Wilson et al., 2018). Ice sheet modelling using the temperature evolution from Antarctic ice cores suggests that a WAIS collapse could have occurred at 405–402 ka after a sustained warming period of the ocean for 4 kyr, contributing 4.3–4.7 m SLE, with a more uncertain contribution from the EAIS of 2.3–3.7 m SLE (Mas e Braga et al., 2021). These results do not consider any potential contribution from the early MIS 11c Antarctic temperature maximum at 426 ka, arising from the bipolar seesaw and Southern Ocean warming.

The long duration of MIS 11c may have also allowed temperate species to reach higher latitudes during their interglacial migration from glacial refugia. A well-documented case is that of the distinctive *Lyrodiscus* molluscan fauna of MIS 11c deposits in Britain (Preece et al., 2007) and France (Limondin-Lozouet and Antoine, 2006). *Lyrodiscus*, a subgenus of land snail now living only on the Canary Islands, has been found in Early and early-Middle Pleistocene deposits, but MIS 11c marks its last occurrence in northwest Europe. While the extensive MIS 12 glaciation would have pushed any remaining refugial populations farther south than previous glacials, the protracted duration of MIS 11c may have allowed *Lyrodiscus* to spread to NW Europe one last time (Preece et al., 2007). Interglacial length would also account for the great diversity of land snail and plant assemblages encountered in MIS 11c tufa deposits in Britain and France, including unusual mixtures of southern and central European elements (Preece et al., 2007). This implies that during subsequent shorter interglacials, species may not have realized their potential distributions because of insufficient time to migrate to higher latitudes.

7. A 'super interglacial'?

Comparison of interglacial intensities over the last 2.8 million years (Myr) in the Lake El'Gygytgyn record led Melles et al. (2012) to characterize MIS 11c as a 'super interglacial', with mean temperature of the warmest month reaching ~6 °C above present, while that of MIS 5e was ~2 °C above present. On the other hand, a spatially-weighted reconstruction of global average surface temperature based on marine records shows that MIS 5e was the warmest interglacial of the last 800 kyr with peak values 1.99 °C above the 0–5 ka average, compared with MIS 11c peak values of 0.57 °C, the second warmest (Snyder, 2016). While MIS 11c SSTs are generally unexceptional in mid-to-high latitudes (Droxler et al., 2003b), they are the second highest in the low-latitudes (Herbert et al., 2010) and highest in West Equatorial Pacific (Lea et al., 2003). Floral and faunal climate reconstructions in Britain show that peak MIS 11c values were similar to peak Holocene values (Candy et al., 2014), a pattern replicated at many other mid-latitude regions (see review by Kleinen et al., (2014)). Reconstructed precipitation values reveal a much wetter MIS 11c compared to present in mid- and high-latitude sites (e.g. Turner, 1970; Field et al., 2000; Preece et al., 2007; Prokopenko et al., 2010; Tarasov et al., 2011;

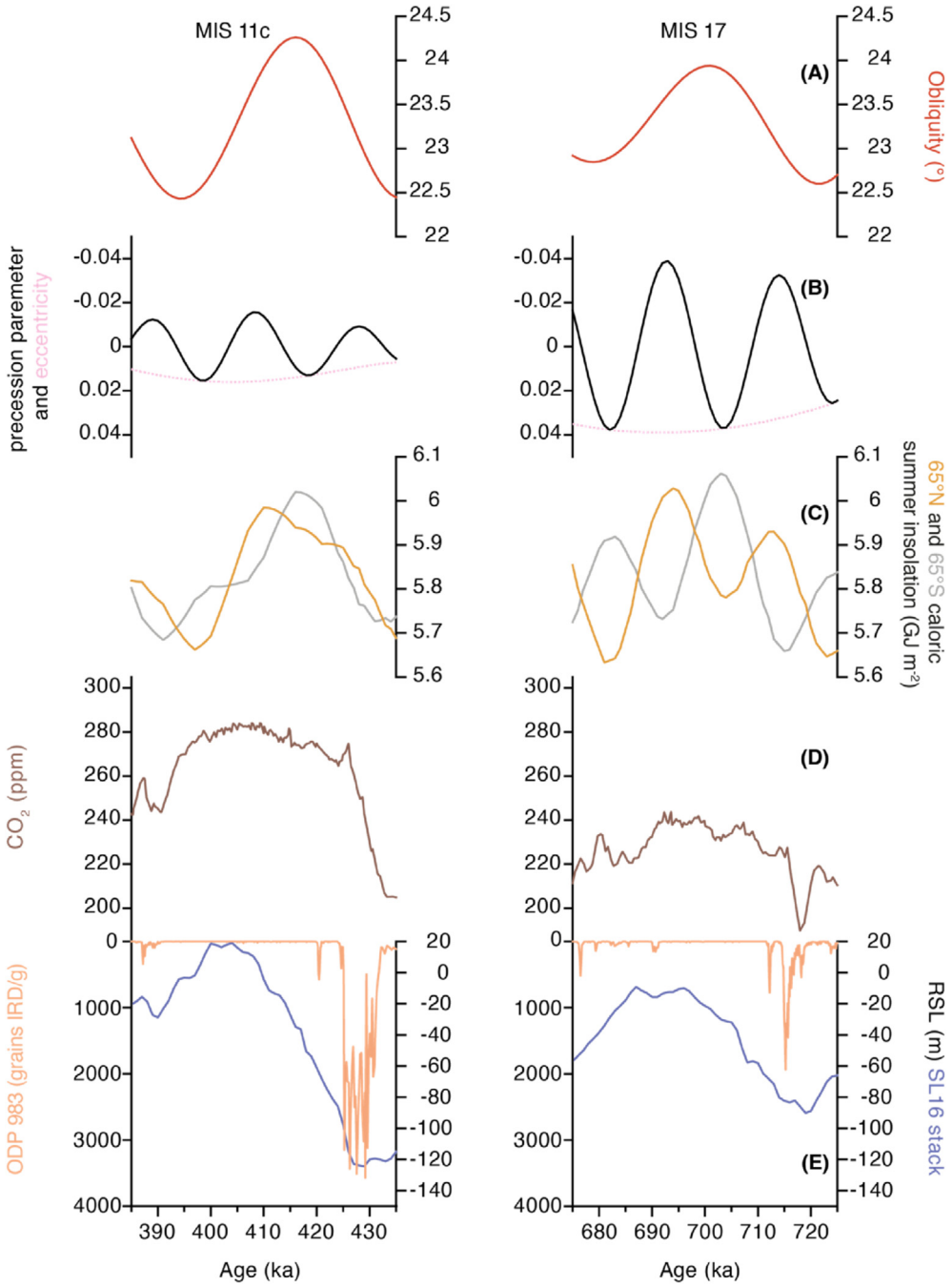

Fig. 7. Comparison of MIS 11c (left) and MIS 17 (right) climatic contexts. A) Obliquity (Laskar et al., 2004). (B) Eccentricity (dashed line) and precession parameter (solid line) (Laskar et al., 2004). (C) Caloric summer half-year insolation at 65°N (orange) and 65°S (grey) (Laskar et al., 2004). (D) Atmospheric CO_2 records (Luthi et al., 2008; Bereiter et al., 2015; Nehrbass-Ahles et al., 2020). (E) Record of ice rafted detritus (IRD) from North Atlantic ODP Site 983 (Barker et al., 2019 [salmon]); relative sea-level (RSL) stack (Spratt and Lisiecki, 2016 [blue]). (For interpretation of the references to colour in this figure legend, the reader is referred to the Web version of this article.)

Melles et al., 2012; Candy et al., 2014). This, combined with increased high-latitude summer temperatures, led to a northward migration of the taiga-tundra boundary (Kleinen et al., 2014). Climate model simulations indicate peak summer temperatures warmer than pre-industrial (Kleinen et al., 2014), but not higher than peak Holocene temperatures (Rachmayani et al., 2016). Apart from certain regions therefore, MIS 11c reconstructed temperature regimes do not support the notion of a 'super interglacial'. Model experiments suggest that combined high summer insolation and concentrations of greenhouse gases contributed to high interglacial intensities in MIS 5e and MIS 9e, while in MIS 11c greenhouse gases contributed to warmth but the subdued summer insolation counteracted this (Yin and Berger, 2012). On the other hand, amplifying feedbacks such as sea-ice reduction (Kleinen et al., 2014) and teleconnections (Melles et al., 2012) may account for strong regional responses.

8. An unusual interglacial

The aphorism 'all interglacials are different but some are more

different than others', may hold a particular resonance for MIS 11c. But in the final analysis, what is special about MIS 11c? Arguably, it has three unusual features: (i) an extended period of decoupling between high CO_2 and high sea level in the part of the interglacial that is unique in the last 800 kyr; (ii) a long duration covering two precession cycles; and (iii) a high sea-level highstand under modest insolation forcing. Some of these features, however, are not unique to MIS 11c. The MIS 17 interglacial (~715–684 ka) also extended over two summer insolation peaks with the obliquity maximum post-dating the first precession minimum by 13 kyr and preceding the second by 8 kyr (but its eccentricity-precession forcing was stronger than that of MIS 11c) (Tzedakis et al., 2012a) (Fig. 7). Reconstructions indicate that sea level also rose gradually in MIS 17, but its highstand was 10 m below present sea level (Spratt and Lisiecki, 2016). In addition, the MIS 17 CO_2 concentration remained relatively stable over a protracted period of ~20 kyr or more, but at substantially lower levels (~230–240 ppm) than MIS 11c. Indeed MIS 17 has the lowest interglacial CO_2 concentration of the last 800 kyr (Bereiter et al., 2015), a key factor to its weak intensity (Yin and Berger, 2012). Extending the MIS 11c – MIS 17 comparison to their preceding glacial maxima reveals a substantial difference in ice volumes (Spratt and Lisiecki, 2016) and supports the idea that instability of the large MIS 12 ice sheets was critical for the subsequent sea-level rise, while the smaller MIS 18 ice sheets may account for the incomplete deglaciation, despite the stronger insolation forcing (see also Fig. 3B). Ice volume differences may have also contributed to the differences in atmospheric CO_2 increase during the MIS 11c and MIS 17 deglaciations: the smaller MIS 18 ice sheets may have led to less salty and less warm AABW formation compared to MIS 12, while weaker meltwater fluxes during Termination VIII (as implied by the smaller and shorter IRD concentrations (Fig. 7E)) led to a more subdued activation of the bipolar seesaw and interhemispheric heat transfer. Both mechanisms would have promoted a lower rate of Antarctic warming and a smaller amount of CO_2 outgassing from the Southern Ocean, which ultimately contributed to the weaker intensity of MIS 17 and its lower sea-level highstand compared to MIS 11c. In addition, unlike MIS 11c, the stronger eccentricity-precession forcing of MIS 17 (Fig. 7B and C) led to a pronounced antiphasing in the rise of caloric summer insolation in the two polar regions, and thus austral summer insolation could not have contributed to the initial melting of sea-ice and CO_2 outgassing at the start of MIS 17. Despite these differences, however, both interglacials show a prolonged sea-level rise (over 20 kyr), with peak highstand attained towards the end of the warm intervals. This was enabled by their long interglacial duration, a function of the precession-obliquity antiphasing, allowing the carbon cycle to maintain relatively stable CO_2 concentrations for over 20 kyr. Indeed, the longer interglacials of the last 1.5 Myr (MIS 11c, 13a, 17, 35, 37, 47, 49) are always associated with the astronomical configuration of the obliquity peak lagging the first precession minimum by 10 ± 2 kyr and leading the second precession minimum by a similar amount. In the case of MIS 11c, the weaker eccentricity also contributed to prolonging the interval of high atmospheric CO_2 levels.

The above considerations suggest that although weak boreal summer insolation forcing (such as at 426 ka) is usually not sufficient to cause substantial sea-level rise, ice sheets at 430 ka had reached a critical size to trigger deglaciation. Sea-level rise was therefore initiated, but at a slow rate due to the weak insolation forcing: the rate was enough to cause substantial CO_2 outgassing, but not enough to lead to a complete loss of Northern Hemisphere ice sheets in one precession cycle. The first weak boreal summer insolation maximum was followed by an obliquity maximum and a weak summer insolation minimum that did not have the power to reverse the sea-level rise and then by a second stronger summer insolation maximum and a further rise in CO_2 due to carbonate compensation. Under these circumstances, the interglacial continued and sea-level rise was completed in the second insolation cycle. Eventually, declining obliquity and boreal summer insolation led to a glacial inception at ~396 ka. If this sequence of events is correct, then the different unusual aspects of MIS 11c are closely connected. The modest boreal summer insolation amplitude means that the conditions for sea-level rise were marginal, leading to the simultaneous presence of large residual ice sheets and high atmospheric CO_2 concentration. However, the weak positive summer insolation forcing also means that it could not be reversed and therefore extended for a long time. And it was the long duration that led to extended warmth and high sea level in the second insolation cycle and allowed processes with a long time constant to gain prominence.

These long-term processes include those of the carbon cycle, where CO_2 concentrations (Nehrbass-Ahles et al., 2020) remained in the range 270–282 ppm for a 24 kyr period (420–396 ka), with multimillennial trends of order 1 ppm/kyr. These conditions were likely the product of a cocktail of counteracting mechanisms, but it is not clear whether the extraordinary stability was accidental or resulted from the operation of stabilizing feedback mechanisms. On the other hand, the intensity of MIS 11c was a function of the high CO_2 concentration attained early in the interglacial. This was related to the duration of AMOC perturbation and Southern Ocean warming, which in turn are partly a function of the large ice sheets of MIS 12. However, such high CO_2 concentrations only occurred after the MBE, so it also seems likely that a fundamental shift of the climate system at that time, allowing more outgassing from the deep ocean than had been possible previously, was also required for MIS 11c to be such a warm interglacial. Transient climate model experiments extending over Termination V and MIS 11c would be valuable in exploring whether terminal processes may have led to a systematic change in post-MBE interglacial state.

Author contributions

P.C. Tzedakis: Conceptualization, Methodology, Writing – original draft, Writing – review & editing, Visualization. D.A. Hodell: Writing – review & editing. C. Nehrbass-Ahles: Writing – review & editing, Visualization. T. Mitsui: Writing – review & editing, Visualization. E.W. Wolff: Conceptualization, Writing – review & editing.

Declaration of competing interest

The authors declare that they have no known competing financial interests or personal relationships that could have appeared to influence the work reported in this paper.

Acknowledgements

We thank Miles Irving for drafting Fig. 4 and Fig. S2. PCT acknowledges funding from the UK Natural Environment Research Council (NE/V001620/1). EWW is supported by a Royal Society Professorship. TM acknowledges funding from the Volkswagen Foundation, Germany. This is a contribution to the PAGES Working Group on Quaternary Interglacials (QUIGS).

Appendix A. Supplementary data

Supplementary data to this article can be found online at https://doi.org/10.1016/j.quascirev.2022.107493.

References

Abe-Ouchi, A., Saito, F., Kawamura, K., Raymo, M.E., Okuno, J., Takahashi, K., Blatter, H., 2013. Insolation-driven 100,000-year glacial cycles and hysteresis of ice-sheet volume. Nature 500, 190–193.

Adkins, J.F., 2013. The role of deep ocean circulation in setting glacial climates. Paleoceanography 28, 539–561.

Archer, D.E., Maier-Reimer, E., 1994. Effect of deep-sea sedimentary calcite preservation on atmospheric CO_2 concentration. Nature 367, 260–263.

Barker, S., Archer, D., Booth, L., Elderfield, H., Henderiks, J., Rickaby, R.E.M., 2006. Globally increased pelagic carbonate production during the Mid-Brunhes dissolution interval and the CO_2 paradox of MIS 11. Quat. Sci. Rev. 25, 3278–3293.

Barker, S., Chen, J., Gong, X., Jonkers, L., Knorr, G., Thornalley, D., 2015. Icebergs not the trigger for North Atlantic cold events. Nature 520, 333–336.

Barker, S., Knorr, G., Conn, S., Lordsmith, S., Newman, D., Thornalley, D., 2019. Early interglacial legacy of deglacial climate instability. Paleoceanogr. Paleoclimatol. 34. https://doi.org/10.1029/2019PA003661.

Barth, A.M., Clark, P.U., Bill, N.S., He, F., Pisias, N.G., 2018. Climate evolution across the mid-Brunhes transition. Clim. Past 14, 2071–2087.

Batchelor, C.L., Margold, M., Krapp, M., Murton, D.K., Dalton, A.S., Gibbard, P.L., Stokes, C.R., Murton, J.B., Manica, A., 2019. The configuration of Northern Hemisphere ice sheets through the Quaternary. Nat. Commun. 10, 3713. https://doi.org/10.1038/s41467-019-11601-2.

Bauska, T.K., Marcott, S.A., Brook, E.J., 2021. Abrupt changes in the global carbon cycle during the last glacial period. Nat. Geosci. 14, 91–96.

Bazin, L., Landais, A., Lemieux-Dudon, B., Kele, H.T.M., Veres, D., Parrenin, F., Martinerie, P., Ritz, C., Capron, E., Lipenkov, V., Loutre, M.F., Raynaud, D., Vinther, B., Svensson, A., Rasmussen, S.O., Severi, M., Blunier, T., Leuenberger, M., Fischer, H., Masson-Delmotte, V., Chappellaz, J., Wolff, E., 2013. An optimized multi-proxy, multi-site Antarctic ice and gas orbital chronology (AICC2012): 120-800 ka. Clim. Past 9, 1715–1731.

Bereiter, B., Eggleston, S., Schmitt, J., Nehrbass-Ahles, C., Stocker, T.F., Fischer, H., Kipfstuhl, S., Chappellaz, J., 2015. Revision of the EPICA Dome C CO_2 record from 800 to 600 kyr before present. Geophys. Res. Lett. 42, 542–549. https://doi.org/10.1002/2014GL061957.

Berger, W.H., Wefer, G., 2003. On the dynamics of the ice ages: stage-11 paradox, mid-Brunhes climate shift, and 100-ky cycle. In: Droxler, A.W., Poore, R.Z., Burckle, L.H. (Eds.), Earth's Climate and Orbital Eccentricity: the Marine Isotope Stage 11 Question, vol. 137. AGU Geophysical Monograph Series, pp. 41–59.

Biller-Celander, N., Shakun, J.D., McGee, D., Wong, C.I., Reyes, A.V., Hardt, B., Tal, I., Ford, D.C., Lauriol, B., 2021. Increasing Pleistocene permafrost persistence and carbon cycle conundrums inferred from Canadian speleothems. Sci. Adv. 7, eabe5799. https://doi.org/10.1126/sciadv.abe5799.

Birchfield, G.E., Weertman, J., Lunde, A.T., 1981. A paleoclimate model of Northern Hemisphere ice sheets. Quat. Res. 15, 126–142.

Blackburn, T., Edwards, G.H., Tulaczyk, S., Scudder, M., Piccione, G., Hallet, B., McLean, N., Zachos, J.C., Cheney, B., Babbe, J.T., 2020. Ice retreat in Wilkes basin of East Antarctica during a warm interglacial. Nature 583, 554–559.

Bock, M., Schmitt, J., Beck, J., Seth, B., Chappellaz, J., Fischer, H., 2017. Glacial/interglacial wetland, biomass burning, and geologic methane emissions constrained by dual stable isotopic CH_4 ice core records. Proc. Natl. Acad. Sci. U.S.A. 114, E5778–E5786.

Bowen, D.Q., 2010. Sea level ~400 000 years ago (MIS 11): analogue for present and future sea-level? Clim. Past 6, 19–29.

Brandon, M., Landais, A., Duchamp-Alphonse, S., Favre, V., Schmitz, L., Abrial, H., Prié, F., Extier, T., Blunier, T., 2020. Exceptionally high biosphere productivity at the beginning of Marine Isotopic Stage 11. Nat. Commun. 11, 2112. https://doi.org/10.1038/s41467-020-15739-2.

Broecker, W.S., Clark, E., McCorkle, D.C., Peng, T.-H., Hajdas, I., Bonani, G., 1999. Evidence for a reduction in the carbonate ion content of the deep sea during the course of the Holocene. Paleoceanography 14, 744–752.

Candy, I., Schreve, D.C., Sherriff, J., Tye, G.J., 2014. Marine Isotope Stage 11: palaeoclimates, palaeoenvironments and its role as an analogue for the current interglacial. Earth Sci. Rev. 128, 18–51.

Cheng, H., Edwards, R.L., Sinha, A., Spötl, C., Yi, L., Chen, S., Kelly, M., Kathayat, G., Wang, X., Li, X., Kong, X., Wang, Y., Ning, Y., Zhang, H., 2016. The Asian monsoon over the past 640,000 years and ice age terminations. Nature 534, 640–646.

Coletti, A.J., DeConto, R.M., Brigham-Grette, J., Melles, M., 2015. A GCM comparison of Pleistocene super-interglacial periods in relation to Lake El'gygytgyn, NE Arctic Russia. Clim. Past 11, 979–989.

Deaney, E.L., Barker, S., van de Flierdt, T., 2017. Timing and nature of AMOC recovery across Termination 2 and magnitude of deglacial CO_2 change. Nat. Commun. 8, 14595.

de Vernal, A., Hillaire-Marcel, H., 2008. Natural variability of Greenland climate, vegetation and ice volume during the past million years. Science 320, 1622–1625.

Dickson, A.J., Beer, C.J., Dempsey, C., Maslin, M.A., Bendle, J.A., McClymont, E.L., Pancost, R.D., 2009. Oceanic forcing of the Marine isotope Stage 11 interglacial. Nat. Geosci. 2, 428–433.

Droxler, A.W., Poore, R.Z., Burckle, L.H. (Eds.), 2003a. Earth's Climate and Orbital Eccentricity: the Marine Isotope Stage 11 Question, vol. 137. AGU Geophysical Monograph Series.

Droxler, A.W., Alley, R.B., Howard, W.R., Poore, R.Z., Burckle, L.H., 2003b. Unique and exceptionally long interglacial marine isotope stage 11: window into Earth warm future climate. In: Droxler, A.W., Poore, R.Z., Burckle, L.H. (Eds.), Earth's Climate and Orbital Eccentricity: the Marine Isotope Stage 11 Question, vol. 137. AGU Geophysical Monograph Series, pp. 1–14.

Dutton, A., Carlson, A.E., Long, A.J., Milne, G.A., Clark, P.U., DeConto, R., Horton, B.P., Rahmstorf, S., Raymo, M.E., 2015. Sea-level rise due to polar ice-sheet mass loss during past warm periods. Science 349, aaa4019. https://doi.org/10.1126/science.aaa4019.

Elderfield, H., Ferretti, G., Greaves, M., Crowhurst, S., McCave, I.N., Hodell, D., Piotrowski, A.M., 2012. Evolution of ocean temperature and ice volume through the Mid-Pleistocene climate transition. Science 337, 704–709.

EPICA community members, 2004. Eight glacial cycles from an Antarctic ice core. Nature 429, 623–628.

Farrell, J.W., Prell, W.L., 1989. Climatic Change and CaCO3 preservation: an 800,000 year bathymetric reconstruction from the central equatorial Pacific Ocean. Paleoceanography 4, 447–466.

Field, M.H., de Beaulieu, J.-L., Guiot, J., Ponel, P., 2000. Middle Pleistocene deposits at La Côte, Val-de-Lans, Isère department, France: plant macrofossil, palynological and fossil insect investigations. Palaeogeogr. Palaeoclimatol. Palaeoecol. 159, 53–83.

Fischer, H., Meissner, K.J., Mix, A.C., Abram, N.J., Austermann, J., Brovkin, V., Capron, E., Colombaroli, D., Daniau, A.-L., Dyez, K.A., Felis, T., Finkelstein, S.A., Jaccard, S.L., McClymont, E.L., Rovere, A., Sutter, J., Wolff, E.W., Affolter, S., Bakker, P., Ballesteros-Cánovas, J.A., Barbante, C., Caley, T., Carlson, A.E., Churakova, O., Cortese, G., Cumming, B.F., Davis, B.A.S., de Vernal, A., Emile-Geay, J., Fritz, S.C., Gierz, P., Gottschalk, J., Holloway, M.D., Joos, F., Kucera, M., Loutre, M.-F., Lunt, D.J., Marcisz, K., Marlon, J.R., Martinez, P., Masson-Delmotte, V., Nehrbass-Ahles, C., Otto-Bliesner, B.L., Raible, C.C., Risebrobakken, B., Sánchez Goñi, M.F., Arrigo, J.S., Sarnthein, M., Sjolte, J., Stocker, T.F., Velasquez Alvárez, P.A., Tinner, W., Valdes, P.J., Vogel, H., Wanner, H., Yan, Q., Yu, Z., Ziegler, M., Zhou, L., 2018. Palaeoclimate constraints on the impact of 2°C anthropogenic warming and beyond. Nat. Geosci. 11, 474–485.

Galaasen, E.V., Ninnemann, U.S., Kessler, A., Irvali, N., Rosenthal, Y., Tjiputra, J., Bouttes, N., Roche, D.M., Kleiven, H.F., Hodell, D.A., 2020. Interglacial instability of North Atlantic deep water ventilation. Science 367, 1485–1489.

Galbraith, E.D., de Lavergne, C., 2019. Response of a comprehensive climate model to a broad range of external forcings: relevance for deep ocean ventilation and the development of late Cenozoic ice ages. Clim. Dynam. 52, 653–679.

Ganopolski, A., Calov, R., 2011. The role of orbital forcing, carbon dioxide and regolith in 100 kyr glacial cycles. Clim. Past 7, 1415–1425.

Ganopolski, A., Brovkin, V., 2017. Simulation of climate, ice sheets and CO_2 evolution during the last four glacial cycles with an Earth system model of intermediate complexity. Clim. Past 13, 1695–1716.

Giaccio, B., Marino, G., Marra, F., Monaco, L., Pereira, A., Zanchetta, G., Gaeta, M., Leicher, N., Nomade, S., Palladino, D.M., Sottili, G., Guillou, H., Scao, V., 2021. Tephrochronological constraints on the timing and nature of sea-level change prior to and during glacial termination V. Quat. Sci. Rev. 263, 106976.

Grant, K.M., Rohling, E.J., Ramsey, C.B., Cheng, H., Edwards, R.L., Florindo, F., Heslop, D., Marra, F., Roberts, A.P., Tamisiea, M.E., Williams, F., 2014. Sea-level variability over five glacial cycles. Nat. Commun. 5, 5076.

Haeberli, M., Baggenstos, D., Schmitt, J., Grimmer, M., Michel1, A., Kellerhals, T., Fischer, H., 2021. Snapshots of mean ocean temperature over the last 700 000 years using noble gases in the EPICA Dome C ice core. Clim. Past 17, 843–867.

Hatfield, R.G., Reyes, A.V., Stoner, J.S., Carlson, A.E., Beard, B.L., Winsor, K., Welke, B., 2016. Interglacial responses of the southern Greenland ice sheet over the last 430,000 years determined using particle-size specific magnetic and isotopic tracers. Earth Planet Sci. Lett. 454, 225–236.

Herbert, T.D., Cleaveland Peterson, L., Lawrence, K.T., Liu, L., 2010. Tropical ocean temperatures over the past 3.5 million years. Science 328, 1530–1534.

Hillenbrand, C.-D., Fütterer, D., Grobe, H., Frederichs, T., 2002. No evidence for a Pleistocene collapse of the West Antarctic ice sheet from continental margin sediments recovered in the Amundsen Sea. Geo Mar. Lett. 22, 51–59.

Hillenbrand, C.D., Kuhn, G., Frederichs, T., 2009. Record of a Mid-Pleistocene depositional anomaly in West Antarctic continental margin sediments: an indicator for ice-sheet collapse? Quat. Sci. Rev. 28, 1147–1159.

Hodell, D.A., Charles, C.D., Sierro, F.J., 2001. Late Pleistocene evolution of the ocean's carbonate system. Earth Planet Sci. Lett. 192, 109–124.

Hodell, D.A., Venz, K.A., Charles, C.D., Sierro, F.J., 2003. The mid-Brunhes transition in ODP sites 1089 and 1090. In: Droxler, A.W., Poore, R.Z., Burckle, L.H. (Eds.), Earth's Climate and Orbital Eccentricity: the Marine Isotope Stage 11 Question, vol. 137. AGU Geophysical Monograph Series, pp. 113–129.

Hodell, D.A., Channell, J.E.T., Curtis, J., Romero, O., Roehl, U., 2008. Onset of "Hudson strait" Heinrich events in the eastern North Atlantic at the end of the middle Pleistocene transition (~640 ka)? Paleoceanography 23, PA4218. https://doi.org/10.1029/2008PA001591.

Holden, P.B., Edwards, N.R., Wolff, E.W., Valdes, P.J., Singarayer, J.S., 2011. The mid-Brunhes event and West Antarctic ice sheet stability. J. Quat. Sci. 26, 474–477.

Hughes, P.D., Gibbard, P.L., 2018. Global glacier dynamics during 100 ka Pleistocene

glacial cycles. Quat. Res. 90, 222–243.
Husson, L., Pastier, A.-M., Pedoja, K., Elliot, M., Paillard, D., Authemayou, C., Sarr, A.-C., Schmitt, A., Cahyarini, S.Y., 2018. Reef carbonate productivity during quaternary sea level oscillations. G-cubed 19. https://doi.org/10.1002/2017GC007335.
Imbrie, J., Imbrie, J.Z., 1980. Modeling the climatic response to orbital variations. Science 207, 943–953.
Imbrie, J., Berger, A., Boyle, E.A., Clemens, S.C., Duffy, A., Howard, W.R., Kukla, G., Kutzbach, J., Martinson, D.G., McIntyre, A., Mix, A.C., Molfino, B., Morley, J.J., Peterson, L.C., Pisias, N.G., Prell, W.L., Raymo, M.E., Shackleton, N.J., Toggweiler, J.R., 1993. On the structure and origin of major glaciation cycles. Part 2: the 100,000-year cycle. Paleoceanography 8, 699–735.
Irvalı, N., Galaasen, E.V., Ninnemann, U.S., Rosenthal, Y., Born, A., Kleiven, H.F., 2020. A low climate threshold for south Greenland Ice Sheet demise during the Late Pleistocene. Proc. Natl. Acad. Sci. U.S.A. 117, 190–195.
Jansen, J.H.F., Kuipers, A., Troelstra, S.R., 1986. A mid-Brunhes climatic event: long-term changes in global atmosphere and ocean circulation. Science 232, 619–622.
Jouzel, J., Masson-Demotte, V., Cattani, O., Dreyfus, G., Falourd, S., Hoffmann, G., Minster, B., Nouet, J., Barnola, J.M., Chappellaz, J., Fischer, H., Gallet, J.C., Johnsen, S., Leuenberger, M., Loulergue, L., Luethis, D., Oerter, H., Parrenin, F., Raisbeck, G., Raynaud, D., Schilt, A., Schwander, J., Selmo, E., Souchez, R., Spahni, R., Stauffer, B., Steffensen, J.P., Stenni, B., Stocker, T.F., Tison, J.L., Werner, M., Wolff, E.W., 2007. Orbital and millennial Antarctic climate variability over the past 800,000 years. Science 317, 793–796.
Kandiano, E.S., Bauch, H.A., Fahl, K., Helmke, J.P., Röhl, U., Pérez-Folgado, M., Cacho, I., 2012. The meridional temperature gradient in the eastern North Atlantic during MIS 11 and its link to the ocean atmosphere system. Palaeogeogr. Palaeoclimatol. Palaeoecol. 333, 24–39.
Kandiano, E.S., van der Meer, M.T.J., Schouten, S., Fahl, K., Sinninghe Damsté, J.S., Bauch, H.A., 2017. Response of the North Atlantic surface and intermediate ocean structure to climate warming of MIS 11. Sci. Rep. 7, 46192. https://doi.org/10.1038/srep46192.
Kleinen, T., Brovkin, V., Munhoven, G., 2016. Modelled interglacial carbon cycle dynamics during the Holocene, the Eemian and marine isotope stage (MIS) 11. Clim. Past 12, 2145–2160.
Kleinen, T., Hildebrandt, S., Prange, M., Rachmayani, R., Müller, S., Bezrukova, S., Brovkin, V., Tarasov, P., 2014. The climate and vegetation of Marine Isotope Stage 11 – model results and proxy-based reconstructions at global and regional scale. Quat. Int. 348, 247–265.
Knorr, G., Barker, S., Zhang, X., Lohmann, G., Xun, G., Gierz, P., Stepanek, C., Stap, L.B., 2021. A salty deep ocean as a prerequisite for glacial termination. Nat. Geosci. 14, 930–936.
Koutsodendris, A., Müller, U.C., Pross, J., Brauer, A., Kotthoff, U., Lotter, A.F., 2010. Vegetation dynamics and climate variability during the Holsteinian interglacial based on a pollen record from Dethlingen (northern Germany). Quat. Sci. Rev. 29, 3298–3307.
Lang, N., Wolff, E.W., 2011. Interglacial and glacial variability from the last 800 ka in marine, ice and terrestrial archives. Clim. Past 7, 361–380.
Laskar, J., Joutel, F., Gastineau, M., Correia, A.C.M., Levrard, B., 2004. A long-term numerical solution for the insolation quantities of the Earth. Astron. Astrophys. 428, 261–285.
Lea, D.W., Pak, D.K., Spero, H.J., 2003. sea surface temperatures in the western equatorial pacific during marine isotope stage 11. In: Droxler, A.W., Poore, R.Z., Burckle, L.H. (Eds.), Earth's Climate and Orbital Eccentricity: the Marine Isotope Stage 11 Question, vol. 137. AGU Geophysical Monograph Series, pp. 147–156.
Limondin-Lozouet, N., Antoine, P., 2006. A new Lyrodiscus (Mollusca, Gastropoda. assemblage from Saint-Acheul (Somme valley): a reappraisal of MIS 11 malacofaunas from northern France. Boreas 35, 622–633.
Lisiecki, L.E., Raymo, M.E., 2005. A Pliocene-Pleistocene stack of 57 globally distributed benthic delta O-18 records. Paleoceanography 20, PA1003. https://doi.org/10.1029/2004PA001071.
Loulergue, L., Schilt, A., Spahni, R., Masson-Delmotte, V., Blunier, T., Lemieux, B., Barnola, J.M., Raynaud, D., Stocker, T.F., Chappellaz, J., 2008. Orbital and millennial-scale features of atmospheric CH_4 over the past 800,000 years. Nature 435, 383–386.
Loutre, M.F., Berger, A., 2000. Future climatic changes: are we entering an exceptionally long interglacial? Clim. Change 46, 61–90.
Loutre, M.F., Berger, A., 2003. Marine Isotope Stage 11 as an analogue for the present interglacial. Global Planet. Change 36, 209–217.
Lüthi, D., Le Floch, M., Stocker, T.F., Bereiter, B., Blunier, T., Barnola, J.M., Siegenthaler, U., Raynaud, D., Jouzel, J., 2008. High-resolution carbon dioxide concentration record 650,000-800,000 years before present. Nature 453, 379–382.
MacAyeal, D.R., 1979. A catastrophe model of the paleoclimate. J. Glaciol. 24, 245–257.
Marcott, S.A., Bauska, T.K., Buizert, C., Steig, E.J., Rosen, J.L., Cuffey, K.M., Fudge, T.J., Severinghaus, J.P., Ahn, J., Kalk, M.L., McConnell, J.R., Sowers, T., Taylor, K.C., White, J.W., Brook, E.J., 2014. Centennial-scale changes in the global carbon cycle during the last deglaciation. Nature 514, 616–619.
Mas e Braga, M., Bernales, J., Prange, M., Stroeven, A.P., Rogozhina, I., 2021. Sensitivity of the Antarctic ice sheets to the warming of marine isotope substage 11c. Cryosphere 15, 459–478.
McManus, J.F., Oppo, D.W., Cullen, J.L., 2003. Marine isotope stage 11 (MIS 11): analog for Holocene and future climate?. In: Droxler, A.W., Poore, R.Z., Burckle, L.H. (Eds.), Earth's Climate and Orbital Eccentricity: the Marine Isotope Stage 11 Question, vol. 137. AGU Geophysical Monograph Series, pp. 69–85.
Melles, M., Brigham-Grette, J., Minyuk, P.S., Nowaczyk, N.R., Wennrich, V., DeConto, R.M., Anderson, P.M., Andreev, A., Coletti, A., Cook, T., Haltia-Hovi, E., Kukkonen, M., Lozhkin, A.V., Rosén, P., Tarasov, P., Vogel, H., Wagner, B., 2012. 2.8 million years of Arctic climate change from Lake El'gygytgyn, NE Russia. Science 337, 315–320.
Milker, Y., Rachmayani, R., Weinkauf, M.F.G., Prange, M., Raitzsch, M., Schulz, M., Kučera, M., 2013. Global and regional sea surface temperature trends during Marine Isotope Stage 11. Clim. Past 9, 2231–2252.
Nehrbass-Ahles, C., Shin, J., Schmitt, J., Bereiter, B., Joos, F., Schilt, A., Schmidely, L., Silva, L., Teste, G., Grilli, R., Chappellaz, J., Hodell, D., Fischer, H., Stocker, T.F., 2020. Abrupt CO_2 release to the atmosphere under glacial and early interglacial climate conditions. Science 369, 1000–1005.
Niu, L., Lohmann, G., Gierz, P., Gowan, E.J., Knorr, G., 2021. Coupled climate-ice sheet modelling of MIS-13 reveals a sensitive Cordilleran Ice Sheet. Global Planet. Change 200, 103474.
Oppo, D.W., McManus, J.F., Cullen, J., 1998. Abrupt climate events 500,000-340,000 years ago: evidence from subpolar North Atlantic sediments. Science 279, 1335–1338.
Paillard, D., 1998. The timing of Pleistocene glaciations from a simple multiple- state climate model. Nature 391, 378–381.
Paillard, D., Parrenin, F., 2004. The Antarctic ice-sheet and the triggering of deglaciations. Earth Planet Sci. Lett. 227, 263–271.
Past Interglacials Working Group of Pages, 2016. Interglacials of the last 800,000 years. Rev. Geophys. 54. https://doi.org/10.1002/2015RG000482.
Peterson, L.C., Prell, W.L., 1985. Carbonate preservation and rates of climatic change: an 800 kyr record from the Indian Ocean. In: Sundquist, E.T., Broecker, W.S. (Eds.), The Carbon Cycle and Atmospheric CO_2: Natural Variations Archean to Present, vol. 32. AGU Geophysical Monograph Series, pp. 251–269.
Pol, K., Debret, M., Masson-Delmotte, V., Capron, E., Cattani, O., Dreyfus, G., Falourd, S., Johnsen, S., Jouzel, J., Landais, A., Minster, B., Stenni, B., 2011. Links between MIS 11 millennial to sub-millennial climate variability and long term trends as revealed by new high resolution EPICA Dome C deuterium data - a comparison with the Holocene. Clim. Past 7, 437–450.
Preece, R.C., Parfitt, S.A., Bridgland, D.R., Lewis, S.G., Rowe, P.J., Atkinson, T.C., Candy, I., Debenham, N.C., Penkman, K.E.H., Rhodes, E.J., Schwenninger, J.-L., Griffiths, H.I., Whittaker, J.E., Gleed-Owen, C., 2007. Terrestrial environments during MIS 11: evidence from the palaeolithic site at west stow, Suffolk, UK. Quat. Sci. Rev. 26, 1236–1300.
Prokopenko, A.A., Bezrukova, E.V., Khursevich, G.K., Solotchina, E.P., Kuzmin, M.I., Tarasov, P.E., 2010. Climate in continental interior Asia during the longest interglacial of the past 500 000 years: the new MIS 11 records from Lake Baikal, SE Siberia. Clim. Past 6, 31–48.
Qin, B., Li, T., Xiong, Z., Algeo, T.J., Jia, Q., 2018. Deep-water carbonate ion concentrations in the western tropical pacific since the mid-pleistocene: a major perturbation during the mid-Brunhes. J. Geophys. Res.: Oceans 123, 6876–6892.
Rachmayani, R., Prange, Schulz, M., 2016. Intra-interglacial climate variability: model simulations of Marine Isotope Stages 1, 5, 11, 13, and 15. Clim. Past 12, 677–695.
Railsback, L.B., Gibbard, P.L., Head, M.J., Voarintsoa, N.R.G., Toucanne, S., 2015. An optimized scheme of lettered marine isotope substages for the last 1.0 million years, and the climatostratigraphic nature of isotope stages and substages. Quat. Sci. Rev. 111, 94–106.
Raymo, M.E., 1997. The timing of major climate terminations. Paleoceanography 12, 577–585.
Raymo, M.E., Mitrovica, J.X., 2012. Collapse of polar ice sheets during the stage 11 interglacial. Nature 483, 453–456.
Reille, M., de Beaulieu, J.-L., Svobodova, H., Andrieu-Ponel, V., Goeury, C., 2000. Pollen analytical biostratigraphy of the last five climatic cycles from a long continental sequence from the Velay region (Massif Central, France). J. Quat. Sci. 15, 665–685.
Reyes, A.V., Carlson, A.E., Beard, B.L., Hatfield, R.G., Stoner, J.S., Winsor, K., Welke, B., Ullman, D.J., 2014. South Greenland ice-sheet collapse during marine isotope stage 11. Nature 510, 525–528.
Ridgwell, A., Maslin, M., Kaplan, J.O., 2012. Flooding of the continental shelves as a contributor to deglacial CH_4 rise. J. Quat. Sci. 27, 800–806.
Robinson, A., Alvarez-Solas, J., Calov, R., Ganopolski, A., Montoya, M., 2017. MIS-11 duration key to disappearance of the Greenland ice sheet. Nat. Commun. 8, 16008. https://doi.org/10.1038/ncomms16008.
Rodrigues, T., Voelker, A.H.L., Grimalt, J.O., Abrantes, F., Naughton, F., 2011. Iberian Margin sea surface temperature during MIS 15 to 9 (580-300 ka): glacial suborbital variability versus interglacial stability. Paleoceanography 26, PA1204. https://doi.org/10.1029/2010PA001927.
Rohling, E.J., Braun, K., Grant, K., Kucera, M., Roberts, A.P., Siddall, M., Trommer, G., 2010. Comparison between Holocene and marine isotope stage-11 Sea-level histories. Earth Planet Sci. Lett. 291, 97–105.
Saavedra-Pellitero, M., Baumann, K.-H., Ullermann, J., Lamy, F., 2017. Marine isotope stage 11 in the pacific sector of the Southern Ocean; a coccolithophore perspective. Quat. Sci. Rev. 158, 1–14.
Shackleton, N.J., 1987. Oxygen isotopes, ice volume and sea level. Quat. Sci. Rev. 6, 183–190.
Schaefer, J.M., Finkel, R.C., Balco, G., Alley, R.B., Caffee, M.C., Briner, J.P., Young, N.E., Gow, A.J., Schwartz, R., 2016. Greenland was nearly ice-free for extended

periods during the Pleistocene. Nature 540, 252–255.
Shakun, J.D., Lea, D.W., Lisiecki, L.E., Raymo, M.E., 2015. An 800-kyr record of global surface ocean $\delta^{18}O$ and implications for ice volume-temperature coupling. Earth Planet Sci. Lett. 426, 58–68.
Shin, J., Nehrbass-Ahles, C., Grilli, R., Chowdhry Beeman, J., Parrenin, F., Teste, G., Landais, A., Schmidely, L., Silva, L., Schmitt, J., Bereiter, B., Stocker, T.F., Fischer, H., Chappellaz, J., 2020. Millennial-scale atmospheric CO_2 variations during the Marine Isotope Stage 6 period (190–135 ka). Clim. Past 16, 2203–2219.
Snyder, C.W., 2016. Evolution of global temperature over the past two million years. Nature 538, 226–228.
Spratt, R.M., Lisiecki, L.E., 2016. A Late Pleistocene sea level stack. Clim. Past 12, 1079–1092.
Stein, R., Hefter, J., Grützner, J., Voelker, A., Naafs, B.D.A., 2009. Variability of surface water characteristics and Heinrich-like events in the Pleistocene midlatitude North Atlantic ocean: biomarker and XRD records from IODP site U1313 (MIS 16-9). Paleoceanography 24, PA2203. https://doi.org/10.1029/2008PA001639.
Tarasov, P.E., Nakagawa, T., Demske, D., Österle, H., Igarashi, Y., Kitagawa, J., Mokhova, L., Bazarova, V., Okuda, M., Gotanda, K., Miyoshi, N., Fujiki, T., Takemura, K., Yonenobu, H., Fleck, A., 2011. Progress in reconstruction of Quaternary climate dynamics in the Northwest Pacific: a new modern-analogue reference dataset and its application to the 430-kyr pollen record from Lake Biwa. Earth Sci. Rev. 108, 64–79.
Turner, C., 1970. The middle Pleistocene deposits at marks Tey, Essex. Phil. Trans. R. Soc. B 257, 373–437.
Tzedakis, P.C., 2010. The MIS 11 – MIS 1 analogy, southern European vegetation, atmospheric methane and the "early anthropogenic hypothesis". Clim. Past 6, 131–144.
Tzedakis, P.C., Hooghiemstra, H., Pälike, H., 2006. The last 1.35 million years at Tenaghi Philippon: revised chronostratigraphy and long-term vegetation trends. Quat. Sci. Rev. 25, 3416–3430.
Tzedakis, P.C., Raynaud, D.R., McManus, J.F., Berger, A., Brovkin, V., Kiefer, T., 2009. Interglacial diversity. Nat. Geosci. 2, 751–755.
Tzedakis, P.C., Wolff, E.W., Skinner, L.C., Brovkin, V., Hodell, D.A., McManus, J.F., Raynaud, D., 2012a. Can we predict the duration of an interglacial? Clim. Past 8, 1473–1485.
Tzedakis, P.C., Channell, J.E.T., Hodell, D.A., Kleiven, H.F., Skinner, L.C., 2012b. Determining the natural length of the current interglacial. Nat. Geosci. 5, 138–141.
Tzedakis, P.C., Crucifix, M., Mitsui, T., Wolff, E.W., 2017. A simple rule to determine which insolation cycles lead to interglacials. Nature 542, 427–432.
Vaks, A., Gutareva, O.S., Breitenbach, S.F.M., Avirmed, E., Mason, A.J., Thomas, A.L., Osinzev, A.V., Kononov, A.M., Henderson, G.M., 2013. Speleothems reveal 500,000-year history of Siberian permafrost. Science 340, 183–186.
Vaks, A., Mason, A.J., Breitenbach, S.F.M., Kononov, A.M., Osinzev, A.V., Rosensaft, M., Borshevsky, A., Gutareva, O.S., Henderson, G.M., 2020. Palaeoclimate evidence of vulnerable permafrost during times of low sea ice. Nature 577, 221–225.
Vázquez Riveiros, N., Waelbroeck, C., Skinner, L., Duplessy, J.-C., McManus, J.F., Kandiano, E.S., Bauch, H.A., 2013. The "MIS 11 paradox" and ocean circulation: role of millennial scale events. Earth Planet Sci. Lett. 371–372, 258–268.
Voelker, A.H.L., Rodrigues, T., Billups, K., Oppo, D., McManus, J., Stein, R., Hefter, J., Grimalt, J.O., 2010. Variations in mid-latitude North Atlantic surface water properties during the mid-Brunhes (MIS 9–14) and their implications for the thermohaline circulation. Clim. Past 6, 531–552.
Wilson, D.J., Bertram, R.A., Needham, E.F., van de Flierdt, T., Welsh, K.J., McKay, R.M., Mazumder, A., Riesselman, C.R., Jimenez-Espejo, F.J., Escutia, C., 2018. Ice loss from the east Antarctic ice sheet during late Pleistocene interglacials. Nature 561, 383–386.
Wolff, E.W., Fischer, H., Fundel, F., Ruth, U., Twarloh, B., Littot, G.C., Gaspari, V., 2006. Southern Ocean sea-ice extent, productivity and iron flux over the past eight glacial cycles. Nature 440, 491–496.
Yin, Q., 2013. Insolation-induced mid-Brunhes transition in Southern Ocean ventilation and deep-ocean temperature. Nature 494, 222–225.
Yin, Q.Z., Berger, A., 2012. Individual contribution of insolation and CO_2 to the interglacial climates of the past 800,000 years. Clim. Dynam. 38, 709–724.
Zhang, X., Lohmann, G., Knorr, G., Xu, X., 2013. Different ocean states and transient characteristics in Last Glacial Maximum simulations and implications for deglaciation. Clim. Past 9, 2319–2333.